Soft Matter

Highly stretchable ionically crosslinked acrylate elastomers inspired by polyelectrolyte complexes

Journal:	*Soft Matter*
Manuscript ID	SM-ART-06-2022-000755.R2
Article Type:	Paper
Date Submitted by the Author:	17-Sep-2022
Complete List of Authors:	Cai, Hongyi; Cornell University, Department of Materials Science and Engineering Wang, Zhongtong; Cornell University, Sibley School of Mechanical and Aerospace Engineering Utomo, Nyalaliska; Cornell University, Vidavsky, Yuval; Soreq NRC, Space Environment Department Silberstein, Meredith; Cornell University, Mechanical and Aerospace Engineering; TE-Cornell University

Journal Name

ARTICLE TYPE

Cite this: DOI: 00.0000/xxxxxxxxxx

Highly stretchable ionically crosslinked acrylate elastomers inspired by polyelectrolyte complexes†

Hongyi Cai,[a] Zhongtong Wang,[b] Nyalaliska W. Utomo,[c] Yuval Vidavsky,[‡b] and Meredith N. Silberstein*[b]

Received Date
Accepted Date

DOI: 00.0000/xxxxxxxxxx

Dynamic bonds are a powerful approach to tailor the mechanical properties of elastomers and introduce shape-memory, self-healing, and recyclability. Among the library of dynamic crosslinks, electrostatic interactions among oppositely charged ions have been shown to enable tough and resilient elastomers and hydrogels. In this work, we investigate the mechanical properties of ionically crosslinked ethyl acrylate-based elastomers assembled from oppositely charged copolymers. Using both infrared and Raman spectroscopy, we confirm that ionic interactions are established among polymer chains. We find that the glass transition temperature of the complex is in between the two individual copolymers, while the complex demonstrates higher stiffness and more recovery, indicating that ionic bonds can strengthen and enhance recovery of these elastomers. We compare cycles to increasing strain levels at different strain rates, and hypothesize that at fast strain rates ionic bonds dynamically break and reform while entanglements do not have time to slip, and at slow strain rates ionic interactions are disrupted and these entanglements slip significantly. Further, we show that a higher ionic to neutral monomer ratio can increase the stiffness, but its effect on recovery is minimal. Finally, taking advantage of the versatility of acrylates, ethyl acrylate is replaced with the more hydrophilic 2-hydroxyethyl acrylate, and the latter is shown to exhibit better recovery and self-healing at a cost of stiffness and strength. The design principles uncovered for these easy-to-manufacture polyelectrolyte complex-inspired bulk materials can be broadly applied to tailor elastomer stiffness, strength, inelastic recovery, and self-healing for various applications.

1 Introduction

Elastomers have been a major industrial product since the vulcanization of rubber was invented[1]. During vulcanization, covalent bonds are created among polymer chains[2,3]. These covalent crosslinks prevent chains from sliding past each other, therefore playing a key role in tuning mechanical properties, including stiffness, toughness and ductility[4]. However, the nature of such covalent connections prohibits the reformation of bonds when they are broken due to mechanical stress[5,6], oxidative aging[7], chemical degradation[8] or other factors. Irreversible breakage limits the resilience and lifetime of elastomers[9]. Additionally, these covalent crosslinks prevent straightforward recycling of elastomers[10].

As an alternative strategy, reversible crosslinks are introduced to polymeric networks to tailor their mechanical properties[11,12]. Typical choices include ionic bonds[13,14], metal-ligand coordination[15–19], hydrogen bonding[20–23], dynamic covalent bonds,[24–27], π-π stacking[28], and cationic-aromatic interactions[29]. Unlike the conventional covalent crosslinks mentioned above, these dynamic linkages are able to reform after they are broken. The scission and reattachment of such bonds allow controlled stress relaxation[30] and high fracture toughness[31,32]. In addition, this reversibility also unlocks a variety of advanced properties, like shape-memory[33–35], self-healing[36–38], recyclability[39,40], strong adhesion[41] with triggered detachment[42], 3D printing[43–45], and surface adaptation[46]. For example, shape-memory materials can be manufactured by using a combination of permanent and reversible bonding networks, where the permanent network "memorizes" the designed shape while the reversible bonding network temporarily holds the alternate shape[34,35,47]. The self-healing process of such elastomers can take place at room temperature[36]. It can also be facilitated by different stimuli, such as elevated temperature[48], light[49], and chemical exposure[50]. For example, Yoshie and coau-

[a] Department of Materials Science and Engineering, Cornell University, Ithaca, New York 14853, United States
[b] Sibley School of Mechanical and Aerospace Engineering, Cornell University, Ithaca, New York 14853, United States. Email: meredith.silberstein@cornell.edu
[c] Robert Frederick Smith School of Chemical and Biomolecular Engineering, Cornell University, Ithaca, NY 14853, United States

† Electronic Supplementary Information (ESI) available: [details of any supplementary information available should be included here]. See DOI: 10.1039/cXsm00000x/

‡ Present address: Space Environment Department, Soreq NRC, Yavne 81800, Israel

Table 1 The charged monomer percentage and elastic modulus of individual copolymers and complexes

Materials	Norminal charge (mol%)	Actual charge (mol%)	Elastic modulus at 0.1 s^{-1} (MPa)
EA20+	4.8	3.2	0.7
EA20-	4.8	2.6	0.8
EA20+/-	4.8	2.8	1.7
EA10+	9.1	6.0	0.8
EA10-	9.1	4.0	0.9
EA10+/-	9.1	4.8	2.3
EA5+	16.7	17.8	0.2
EA5-	16.7	15.8	1.3
EA5+/-	16.7	16.8	5.9
HEA5+	16.7	14.5	0.4
HEA5-	16.7	15.6	0.7
HEA5+/-	16.7	15.0	1.1

thors mended a poly(ethylene adipate) network constructed by Diels–Alder (DA) reactions at 60 °C[48]. Ji et al. fabricated polyurethane with dynamic diselenide bonds and induced self-healing behavior with visible light or 457 nm laser[49]. Miwa and coworkers reported one ionically crosslinked elastomer that can be softened and can quickly self-heal in the presence of CO_2 gas[50]. Soft materials with the above characteristics have been applied to energy storage[51,52], soft robotics[53,54], wearable electronics[55], and tissue engineering[56,57].

Ionic bond-based dynamic polymer networks are built by electrostatic interactions between oppositely charged species. These ionic bonds can be found in both hydrogels[58–62] and elastomers[63–65]. Sun et al. fabricated hydrogels based on polyampholytes, polymers bearing both cationic and anionic groups, and the materials demonstrate high toughness, self-healing and viscoelasticity[58]. Later, polyelectrolyte complexes (PECs) are introduced in hydrogel fabrication, which are formed by mixing polycations and polyanions in solution[59]. In addition to the mentioned mechanical properties of polyampholyte and PEC hydrogels, these materials also demonstrate saloplasticity[66–70], meaning they can be softened with salt doping, which enables 3D printing[44]. Luo and coworkers successfully dissolved PECs in NaCl solution and reprocessed them into films, sheets, fibers, and capsules[60]. Mixing of cationic and anionic polymers has also been used in PDMS-based elastomers[63,71]. A recent work by Zheng et al. demonstrates high mechanical strength and thermal reprocessing for silicone-based elastomers bonded with Gemini (double ionic) crosslinks[64].

Inspired by PECs[68,72–76], in this paper we introduce acrylate-based elastomers crosslinked with ionic functionality, which show both viscoelasticity and self-healing properties and sustain large deformation. We choose acrylates as our monomer system because this requires only simple chemistry (free radical polymerization here) yet provides the opportunity for more complicated architectures (e.g. via controlled polymerization). In this work, we synthesized copolymers with both neutral and charged components. The neutral component provides rubbery properties while the charged component forms crosslinks. Acrylates contain a large library of monomers and enable tuning properties by changing the ratio of neutral to charged monomers or by switching the monomer type. We first verify the existence of ionic crosslinks by vibrational spectroscopies, followed by demonstrating that stiffness and recovery under cyclic loading are both enhanced by these ionic bonds. Then we take advantage of the versatility of acrylates, to investigate the effect of crosslink density and different neutral monomer species on mechanical response and self-healing behavior. This work will add understanding of structure-function relationships for ionically-crosslinked polymeric elastomers, with a focus on tunable mechanical properties including recovery. It will also broaden the path to future high-performing elastomers.

2 Results and Discussion

Ethyl acrylate (EA) copolymers were synthesized by free radical polymerization. We adapt a reported procedure for copolymerization of sodium 4-styrenesulfonyl(trifluoromethylsulfonyl) imide and EA[77], instead using [2-(acryloyloxy)ethyl]trimethylammonium chloride (ATMAC) for the cationic copolymers and 3-sulfopropyl acrylate potassium (SPAP) for the anionic copolymers (Figure 1a, SI Section 1). Each copolymer went through dialysis to be purified. For convenience, we name each copolymer according to its neutral monomer identity, target ratio of neutral to charged monomer, and whether it has positive or negative charge. For example, the cationic copolymer with an ingredient monomer ratio EA:ATMAC = 5:1 is EA5+, and the anionic copolymer with an ingredient monomer ratio EA:SPAP = 5:1 as EA5-. The actual ionic component ratios of EA20+, EA10+, EA5+ and EA5- were characterized by ^{1}H nuclear magnetic resonance (^{1}H-NMR, Figure S1-S3, S5), while the ratios of EA20- and EA10- were determined from x-ray photoelectron spectroscopy (XPS) (Table S3) due to poor signals of ionic functionality in these polymers from ^{1}H-NMR. It is worth noting that our individual copolymers fall in the classification of ionomers[78] with their relatively low ionic ratio. To assemble the complex, EA5+ and EA5- were mixed at a ratio such that both copolymers contain the same amount of ionic functionality (*i.e.* more EA5- than EA5+), followed by a second dialysis to remove the counterions (Figure 1b). The obtained material is named EA5+/-. Likewise, EA10+/- and EA20+/- were formed from mixing EA10+ and EA10-, and EA20+ and EA20-, respectively. It is worth noting that after the first dialysis, the individual components of the complex are still fully dissolved within the dialysis tubing, while after the second dialysis, the complex is a white rubbery solid, suggesting that ionic crosslinking has occurred between the oppositely charged polymers. To demonstrate the removal of counterions during complexation, we measured the conductivity of individual copolymers and the complex,

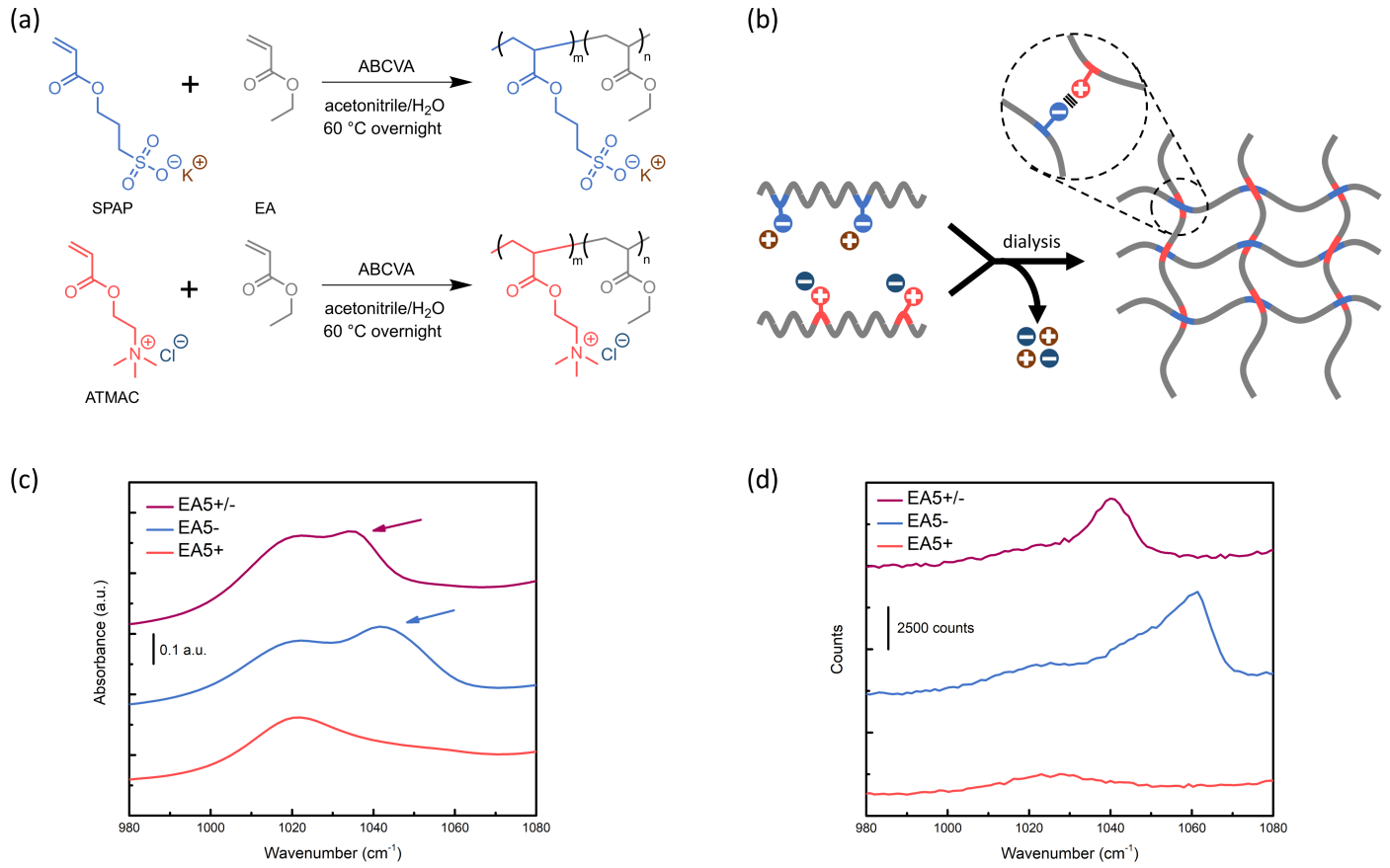

Fig. 1 (a)Scheme for synthesis of anionic and cationic EA-based copolymer using 4,4'-azobis(4-cyanovaleric acid) (ABCVA) as the initiator. (b)Scheme showing complex assembly from two oppositely charged copolymers. The copolymers are first mixed, followed by dialysis to remove the counter-ions from the complex. Ionic crosslinks are formed inside the material. (c)Comparison of FTIR spectra of the complex and the individual components in the 980-1080 cm^{-1} range. The peaks indicated with arrows correspond to the symmetric vibration of the SO_3^- group. The peak position moves to a lower wavenumber when the complex is formed. (d)Raman spectroscopy comparison of the complex and the individual components over the same range. The peaks shown also correspond to the S=O bonds in the SO_3^- group, with the complex peak located at a lower wavenumber position.

which can be a rough estimate of mobile ion concentration. The conductivity of EA20+ is 8.38×10^{-8} S · m^{-1}, EA20- is 6.27×10^{-8} S · m^{-1}, and EA20+/- is 2.14×10^{-9} S · m^{-1}.This indicates that the complex has an ion concentration much lower than the individual components. Elemental analysis (Table S4) also shows that most counterions have been removed. The specimens were stored at a relative humidity of 54% prior to testing, since hydration can act as a plasticizer[79]. The water content by mass of EA20+, EA20-, EA20+/-, EA10+/- and EA5+/- is 2.8%, 2.0%, 1.7%, 2.3%, and 4.9%, respectively.

To find evidence of ionic crosslinks within the complex, Fourier-transform infrared (FTIR) spectroscopy and Raman spectroscopy were used to characterize both the individual components and the complex. In the shown FTIR spectra (Figure 1c), both EA5+/- and EA5- have two peaks while EA5+ only has one. The higher-wavenumber peak is associated with the symmetric vibration of the SO_3^- functionality[80]. This peak redshifts from 1042 cm^{-1} in EA5- to 1034 cm^{-1} in EA5+/-. This shift marks the local chemical environment change around the SO_3^- functionality, which is likely due to potassium being replaced by quaternary ammonium during the complex formation. The ionic crosslinking can also be confirmed from Raman spectroscopy (Figure 1d). Both EA5+/- and EA5- have a sharp peak corresponding to the S=O bonds in the SO_3^- groups[81] in the displayed region while it is absent in EA5+. This peak redshifts from 1061 cm^{-1} in EA5- to 1041 cm^{-1} in EA5+/-. Both spectroscopy characterizations show local environment change near the SO_3^- groups, indicating that there are ionic bonds between the cationic and anionic copolymers during the complex formation.

Next, thermal and mechanical properties are compared among the individual components and the complexes using the 1:20 set of materials. We first investigate the glass transition temperature (T_g) with differential scanning calorimetry (DSC, Figure 2a). The complex has a T_g of -5.10 °C, in between that of the positive component (-5.95 °C) and the negative component (-3.07 °C). For reference, the homopolymer T_g for EA is -23 °C[82], for poly(sodium 4-styrene sulfonate) (PSS, polymers with SO_3^- groups) is 180 °C[83] and for poly-(diallyldimethylammonium chloride) (PDADMAC, polymers with quaternary ammonium) is 166 °C[84] from DSC. The T_g of our EA-based copolymers is significantly lower than those of ionic homopolymers while higher than that of EA, which is a typical characteristic of copolymers[85]. While the EA homopolymer is a sticky and highly viscous fluid, the copolymers and the complexes are rubbery solids. We also studied

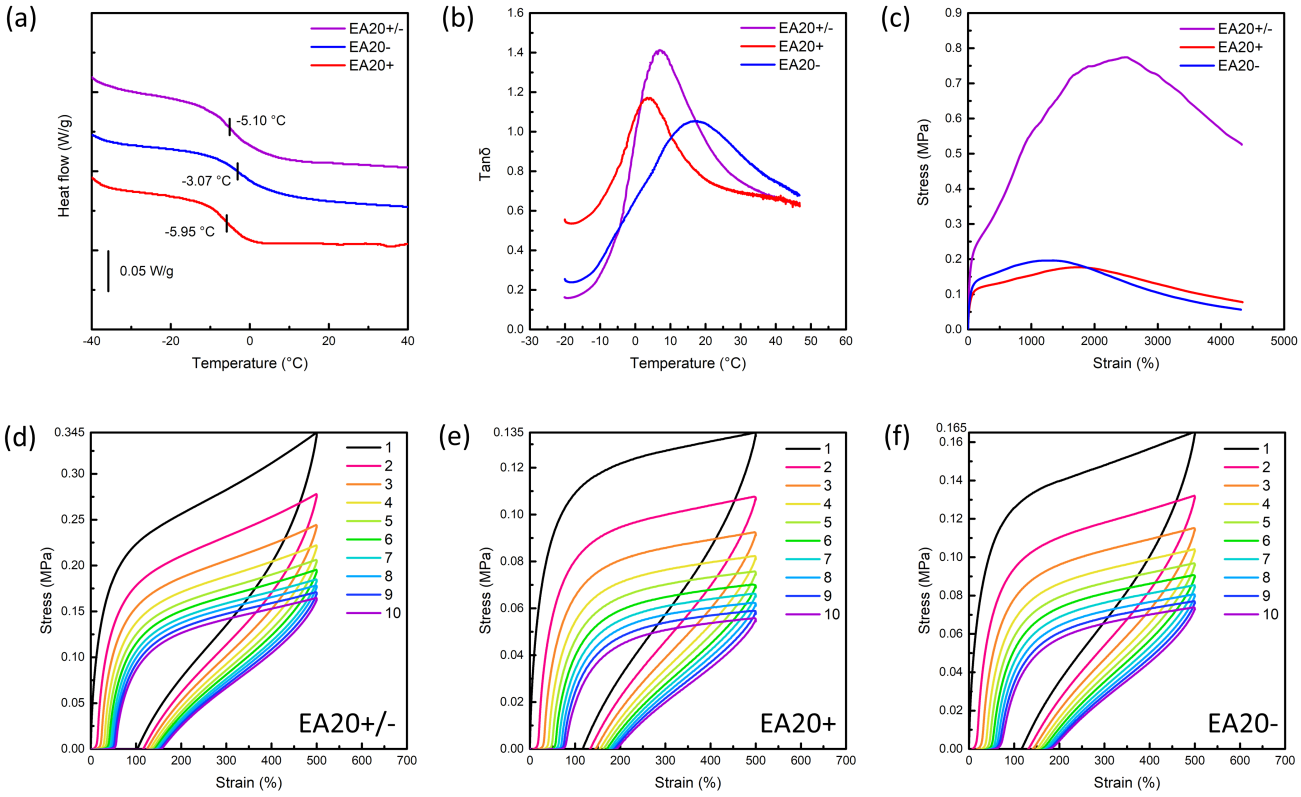

Fig. 2 Comparison between the complex and the individual components. (a)Heat flow curves of the second heating scans with "exotherm up" for the complex and the individual components from DSC. (b)Temperature dependence of tanδ from DMA. Both DSC and DMA indicate the T_g of the complex is in between those of the individual components. (c)Stress-strain curves obtained from monotonic tensile tests at a 0.1 s^{-1} strain rate, with the complex being much stronger while as stretchable as the individual components. (d-f)Repeated cyclic tensile test results for (d)the complex, (e)the cationic component and (f)the anionic component, at a strain rate of 0.1 s^{-1}, with a 10 min wait time between cycles.

the thermo-mechanical properties by dynamic mechanical analysis (DMA), since this technique tends to give results more related to mechanical properties (Figure 2b). The tanδ of both the individual components and the complex show a single peak, indicating minimal phase separation within these copolymers. From DMA results, the complex has a T_g at 7 °C, also in between that of the positive component (4 °C) and the negative component (17 °C). This intermediate T_g means that difference we see in the subsequent stress-strain curves between the individual components and the complex are not due to a T_g shift.

Next, the three materials were subjected to large deformation monotonic tension at constant strain rate (0.1 s^{-1}) (Figure 2c). For all tensile testing, we used rectangular specimens of width 4 mm and thickness approximately 1 mm, with an initial grip-to-grip distance of 20 mm. All results are reported in terms of engineering stress and engineering strain, referred to from here on as simply stress and strain. Force data was converted to engineering stress by divided by initial cross-sectional area. The crosshead displacement was converted to engineering strain by divided by the initial grip-to-grip distance. The three materials have similarly shaped stress-strain curves: an initial linear elastic regime, followed by a strain hardening stage, and after reaching the maximum stress, all three elastomers soften monotonically but remain intact, exceeding 4000% engineering strain, which corresponds to the travel limit of the tensile machine. At such large deformation, the materials demonstrate a clear decrease in width and thickness. Ionomers are known to improve strength and toughness compared to homopolymers[78]. For example, in sulfonated polystyrene (SPS) a low ion content (less than ca. 4 mol%) can increase the tensile strength by 17% and the toughness by 38%, while a higher ion content of about 8 mol% can boost the tensile strength by 57% and the toughness by 100%[86]. Similar effects on mechanical properties can be also seen in polyurethanes[87]. This is also true for our ionomers considering the transformation from a highly viscous fluid homopolymer to a rubbery solid ionomer with an ion content of ca. 3 mol%. Quantitatively, there are significant differences between the complex and the individual components. First, the stiffness of the complex is 1.7 MPa, significantly higher than the stiffness of either of the individual components, the cationic one being 0.7 MPa and the anionic one being 0.8 MPa. For reference, poly(ethyl acrylate) with an Mn of 120 kg/mol shows a storage plateau modulus of 2.2×10^5 Pa at 291 K[88]. Second, the maximum engineering stress and the strain hardening slope are also higher for the complex (0.8 MPa vs. 0.2 MPa for the cationic and the anionic ones). It is clear that the attractive ionic interactions among polymer chains enhance the overall stiffness and strength of the complex, without seriously diminishing the ability to be stretched as typically results from

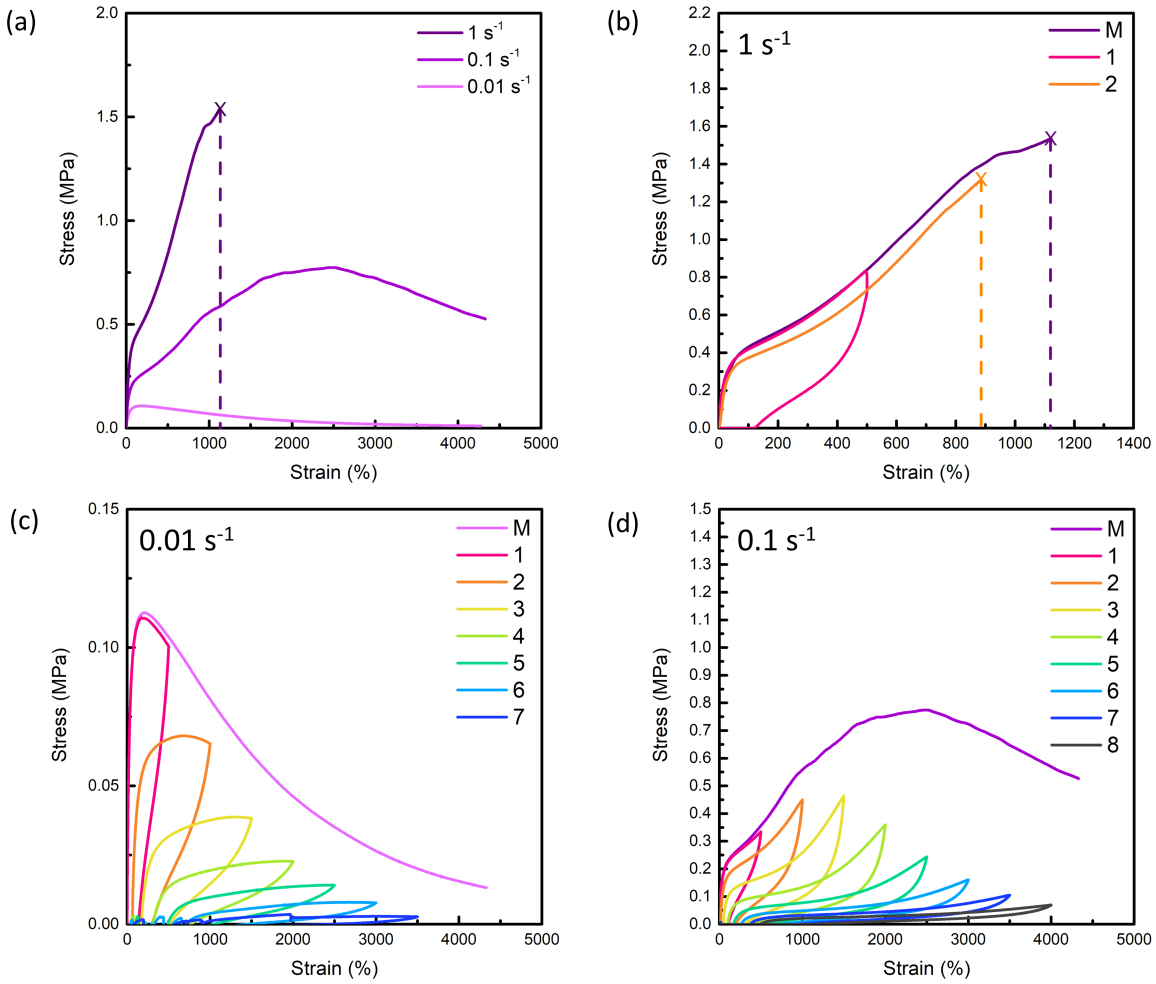

Fig. 3 Mechanical strain rate sensitivity of EA20+/-. (a)Stress-strain curves of monotonic tensile tests obtained at three different strain rates. (b-d)Cyclic tensile loading with an increasing strain at (b)1 s^{-1}, (c)0.01 s^{-1} and (d)0.1 s^{-1}. M stands for monotonic testing to failure. These display that the recovery behavior can significantly change at different strain rates.

covalent crosslinking. Third, the onset of softening is at slightly larger strains for the complex than the two individual components, which likely results from the ionic bonds delaying the relative flow of polymer chains. Finally, the toughness of EA20+/- appears to me much larger than that of EA20+ and EA20-, with the area under the stress-strain curve over the range of strain we tested increasing by 345%.

To investigate the inelastic recovery after mechanical loading, EA20+/-, EA20+, and EA20- were subjected to multiple repeated cyclic tensile loading tests to a strain of 500% with a hold time of 10 min between cycles (Figure 2d-f). Interestingly, the unloading stress-strain curves are similar in shape for all three materials. The complex recovers a larger fraction of energy upon unloading than the two components (44% vs. 40% for both the anionic and the cationic) and also reaches a smaller residual strain (104% vs. 117% for the anionic and 118% for the cationic). After reaching zero force upon unloading, the thin specimen bends and continues to recover as the grips move to their initial position and hold for 10 min. Upon reloading, all three materials show incomplete strain recovery, a reduced elastic modulus, and reduced rollover stress and peak cycle stress. The residual strain upon unloading and residual strain upon reloading continue to increase with cycle number, and the elastic modulus and strength continue to decrease with cycle number. The polymers exhibit a shakedown behavior[89] with the load and unload curves for all three materials approaching a similar and stable shape as the cycle number increases. Residual strain at the beginning of each cycle, stress at the maximum strain of each cycle and modulus were extracted from the plot as parameters to quantitatively analyze the recovery (Figure S7). The complex exhibits less accumulation of residual strain than the individual components. At the start of the 10th cycle, the complex has 57% residual strain, while the cationic and the anionic components have 81% and 77%, respectively. Similarly, the decay in stress and modulus is smaller for the complex. These observations suggest that the ionic interactions between the polymer chains of opposite charge improve the recovery of the material.

One interesting characteristic of materials with dynamic

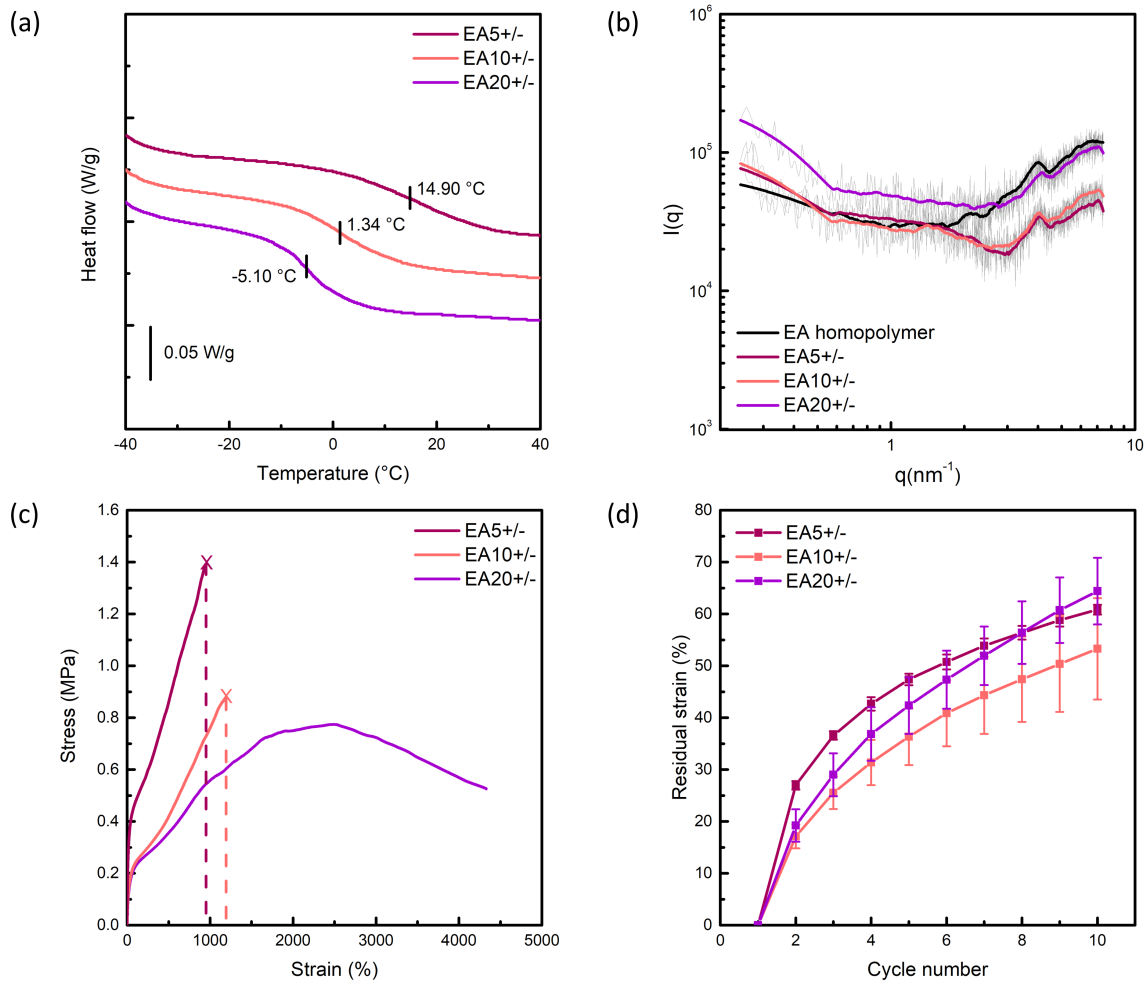

Fig. 4 Comparison of complexes with different ratios of charged to neutral monomers within the polymers. (a)Heat flow curves of the second heating scans with "exotherm up" obtained by DSC. As the crosslink density increases, T_g increases and the glass transition regime grows wider. (b) I(q) vs. q plot from SAXS of the three EA complexes and the EA homopolymer. The solid line is a smoothed version of the original data using 100 pt SG smoothing. A single shared peak at 4 nm^{-1} is observed. (c)Stress-strain curves obtained from monotonic tensile tests at a 0.1 s^{-1} strain rate. The 1:5 and 1:10 complexes fracture while the 1:20 one softens. (d)Residual strain upon reloading of each cycle from repeated cyclic tensile tests at a 0.1 s^{-1} strain rate. The difference in recovery is similar.

crosslinks is the strain-rate dependence of the mechanical properties[58,90–93]. Since our complexes contain attractive ionic interactions among the polymer chains, which can dynamically break and reform, we anticipated that they should also exhibit significant strain rate dependence. Monotonic tensile tests were performed on EA20+/- at three different strain rates (Figure 3a). The strain rate affects both the shape of the curve and the values of the modulus, maximum stress, etc. At the slowest strain rate, 0.01 s^{-1}, the complex reaches a small maximum engineering stress of around 0.1 MPa at a strain of 204%, and then the stress decreases monotonically and approaches zero. Visually, the material stays intact past 4000% strain. At a fast strain rate, 1 s^{-1}, the complex becomes stiff and solid-like. It has an elastic regime and the strain hardening stage, similar to the previously discussed curve at 0.1 s^{-1}, but the slopes are steeper, and the softening is absent, with the complex instead breaking. Still, at such a fast strain rate, the material is quite stretchable, reaching a maximum engineering strain of around 1100%. The moduli at the three strain rates (0.01 s^{-1}, 0.1 s^{-1} and 1 s^{-1}) are 0.8 MPa, 1.7 MPa and 2.0 MPa, respectively. We expect that this strain rate dependence arises from dynamic ionic interactions among the polymer chains in the complex as well as physical entanglements.

We also conducted cycles to increasing strain levels and compare those with the monotonic stress-strain curves at each strain rate in order to better understand the mechanisms governing each strain rate (Figure 3b-d). This experiment reveals a rather interesting characteristic of the material. At the fastest rate, the reloading curve is nearly identical to the monotonic curve, with only a slight drop in rollover stress and an early onset of failure (Figure 3b). This similarity is despite a clearly inelastic unloading curve resulting in significant residual strain prior to the 10 min stress free hold period. Clearly whatever interactions were

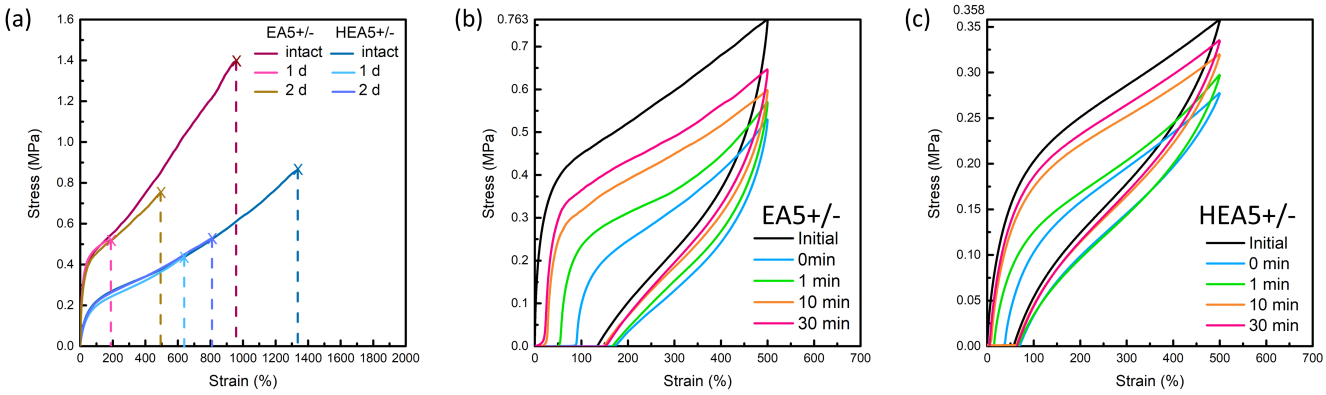

Fig. 5 Comparison of mechanical properties for HEA vs. EA. HEA is more hydrophilic while EA is more hydrophobic. (a)Stress-strain curves obtained from monotonic tensile tests of virgin and self-healing samples with different healing time. The HEA samples are less strong but heal somewhat better. (b,c)Cyclic tensile stress-strain curves of (b)EA and (c)HEA for different waiting times at a 0.1 s^{-1} strain rate. For each type of material, curves are obtained from double cycles with different waiting time in between the first and second using fresh specimens. The initial cycle is the first cycle (using results of 10 min waiting time as representation), and cycles labeled with waiting time are the second cycles. Full results can be found in Figure S11.

disrupted during loading, were able to nearly fully recover during the 10 minutes. We hypothesize that at this fastest rate, ionic bonds can break and reform, but that entanglements mostly do not have time to slip, leaving a crosslink-like memory of the initial material configuration. At the slowest rate, the material starts softening by a strain of 200%, reaching a stress less than 12% of its peak by 4000% strain. (Figure 3c). Here, the second and subsequent loading curves are substantially below the initial loading in terms of stiffness and strength. Unlike in the fast rate test, the residual strain does not recover back to zero before the second cycle, even though the hold time is the same, suggesting that the complex loses more of its memory under this slower loading, and likely experiences significant entanglement slip in addition to disruption of ionic interactions. While this entanglement slip is likely substantial at this rate even in the monotonic case, the greater duration of the load history for the cyclic loading sequence will enhance it further. The intermediate strain rate actually has the greatest difference between the monotonic and cyclic stress-strain curves (Figure 3d). We believe that this is because the extra cycles provide more time at intermediate stress values for disruption of ionic interactions and entanglement slip, compared to the monotonic test. Finally, we conduct cyclic tests for each strain rate to a constant strain of 500% with a 10 minute hold time in between, analogous to the experiments in Figure 2d-f (Figure S8). Up to this strain level, which is prior to significant softening, the fastest rate is more similar to the initial loading, followed by the middle rate, and then the slowest strain rate. For quantitative analysis, the residual strain of cycles at 0.01 s^{-1} increases the most, followed by those at 0.1 s^{-1} and 1 s^{-1}. The 0.01 s^{-1} tests also have the most decay in strength and modulus. These results indicate better recovery of the EA complexes at a faster strain rate.

Next, the effect of the ratio of ionic to neutral functionality is studied. DSC (Figure 4a) shows increasing T_g as the crosslink density increases, from -5.10 °C for EA20+/- and 1.34 °C for EA10+/- to 14.90 °C for EA5+/-. One thing worth noticing is that the temperature range of the glass transition regime grows wider as the ionic ratio increases. DMA tanδ vs. temperature plots (Figure S9a) also show a widened peak for EA10+/- compared to EA20+/-, and the EA5+/- curve barely exhibits a peak. Both results indicate the existence of more complicated dynamics for complexes with higher ratio of ionic functionality. Small angle X-ray scattering (SAXS) data of the three EA complexes and the EA homopolymer (Figure 4b) was gathered to investigate whether the broadening transition seen in both DSC and DMA are caused by domain formation as the ionic ratio increases. All four materials share a peak at 4 nm^{-1}, which corresponds roughly to a length between one to two carbon-carbon single bonds if spherical scattering elements are assumed. The low q upturn observed for all four materials is typically attributed to structural inhomogeneities on larger length scales[94]. We observe a steeper decline in scattering intensity as q increases for EA10+/- and EA5+/- than EA20+/- in the 1.4 nm^{-1} to 2.6 nm^{-1} region, suggesting that there are larger inhomogeneities in the two complexes with higher ionic content than for the third. A Kratky plot of the data (Iq^2 vs q, Figure S13) also illustrates the shared peak at 4 nm^{-1} and the lack of defined peak in the low q regime indicates that all samples are inherently disordered[95]. Scattering from the complexes are not conclusively different, and we believe there is no domain formation in our materials.

Stress-strain curves obtained from monotonic tensile tests (Figure 4c) show significant differences for EA complexes as a function of ionic functionality fraction. Most notably, the 1:5 and 1:10 complexes fracture rather than soften. A higher ionic functionality fraction results in a larger modulus (5.9 MPa and 2.3 MPa for 1:5 and 1:10, respectively vs 1.7 MPa for 1:20) and maximum stress (1.4 MPa and 0.9 MPa vs 0.8 MPa for 1:20), matching the expected trend from the T_g change. The ability to be stretched is also restricted by the greater ratio of ionic functional groups, with the maximum engineering strain being 953% for 1:5 and 1195% for 1:10. These fracture strains are both lower than even the onset of softening for the 1:20 polymer complex. It is shown here that the larger number of ionic interactions enhances stiff-

ness and strength of the complexes, but also limits the strain to failure, which matches our expectation for crosslinks, regardless of traditional covalent or dynamic ones. Inelastic recovery was again investigated through repeated cyclic tensile tests (Figure S9). The shapes of the load-unload cycles look similar for the three different ionic ratios. Unexpectedly, the ability to recover is quite similar for complexes with different ionic bond density. For the first few cycles EA5+/- has the greatest residual strain upon reloading, followed by EA20+/- and EA10+/- (Figure 4d). However, by the eighth cycle the residual strain of all three materials is within experimental error. For normalized strength and modulus (Figure S9d,e), the plots for the three materials similarly overlap. We hypothesize that while a higher ratio of ionic to neutral monomers provides more sites for the bonds to reform, it also restrains the chain configurations from changing relative to each other, making it harder to coil back. It has been shown that, in polyelectrolyte multilayer (PEM) films, charged polymer chains will uncoil under tension[96]. Water uptake is also observed during stretching in PEM, which could be due to water bound directly to charged molecules, showing transient ionic crosslink disruption.[97] The complexity of structures suggested by DSC and DMA could also be a factor. These competing mechanisms diminish the possibility to see a dramatic recovery difference among the three complexes.

As we discussed in the introduction, one reason to use acrylates is that it is easy to find monomer candidates in this family, making it simple to modify the polymer structure. To exhibit the versatility of our strategy, we synthesized ionic copolymers using a different neutral monomer, 2-hydroxyethyl acrylate (HEA). The homopolymer of HEA has a T_g at -14 °C[82], similar to that of EA, while the hydroxyl group introduces hydrophilicity to the polymer. We anticipated that the HEA-based complex would show faster recovery, as the more hydrophilic material may absorb more water from the atmosphere, increasing polymer chain mobility. The stiffness and strength of the material should decrease since water acts as a plasticizer. The synthesized HEA5+ and HEA5- have similar ionic ratios as EA5+ and EA5- (Figure S4, S6). The water content of EA5+/- is 4.9% and HEA5+/- is 8.7% by mass when both are equilibrated in atmosphere at a relative humidity of 54%. A screening effect from the counterions can be seen with our HEA5 copolymers. HEA5+ and HEA5- were separately dissolved in an 0.5 M aqueous solution of KCl. When the two solutions were mixed, the product was still a transparent, colorless solution without precipitation. As expected, the HEA-based complexes show decreased stiffness and strength compared to the EA-based complexes at the same ionic ratio, and the recovery is faster. From both DSC and DMA, the T_g of HEA5+/- is lower than EA5+/- (Figure S10a,b). Under monotonic loading (Figure 5a), the stiffness for HEA5+/- is 1.1 MPa while that of EA5+/- is 5.9 MPa. Recovery was investigated both through self-healing tests and cyclic tests with varied hold times at zero stress. The self-healing properties of the complexes were investigated by cutting the samples into two pieces, reattaching them at the cut surface, placing them in a rectangular mold of their original size, and then subjecting them to monotonic tensile testing after waiting for a set time. Both EA and HEA show good recovery from the damage after reattachment and waiting for two days at room temperature. EA heals to slightly over half the maximum engineering strain while HEA recovers over 60%. Both materials fail at the cut surface. At one day, there is a greater difference between the two materials with HEA recovering 47% and EA recovering only 20%, reflecting the greater HEA mobility. Under cyclic tensile tests with varied waiting time it is again clear that as intended, the HEA complexes have a faster pace of recovery (Figure 5b,c). After 30 min, HEA recovers 94% of its strength while EA recovers only 85%. The unloading curves of HEA5+/- are closer to the corresponding loading/reloading ones than EA5+/-. Cyclic tensile tests with the same waiting time also support the argument of greater recovery for HEA vs EA (Figure S10c-f).

3 Conclusions

In this work, we explored the mechanical properties of ionically crosslinked acrylate-based elastomers assembled from two oppositely charged copolymers, including stiffness, strength, recovery, and self-healing. We first confirmed the existence of ionic interactions in our elastomers using FTIR and Raman spectroscopy, where we find redshift of the SO_3^- functional group. Next, through DSC and DMA we recorded that the T_g of the complex is in between the two individual components, but the complex has higher stiffness and shows more recovery, which indicates the strengthening and recovering effect of ionic bonds in the elastomer. We then navigated the mechanical strain rate dependence of our complexes, reaching a conclusion that higher strength and better recovery can be obtained at faster strain rates. Comparing cycles to increasing strain levels to monotonic stress-strain curves, we draw a picture that at fast strain rates ionic bonds dynamically break and reform while entanglements do not have time to slip, and at slow strain rates ionic interactions are disrupted and these entanglements slip significantly. Following this, we discovered that a higher density of ionic crosslinks can increase T_g and stiffness, but its effect on recovery is minimal. We attribute this to two competing factors, the number of sites for ionic bonds to reform and restraint of chain configuration due to these bonds. Finally, we compared the mechanical response between more hydrophilic and more hydrophobic elastomers, showing that a water content difference of $\sim 4\%$ can help with recovery and self-healing, but at a cost to stiffness and strength. The design principles uncovered here for these easy to manufacture bulk materials formed from mixing oppositely charged chains, can be broadly applied in the future to tailor elastomer stiffness, strength, inelastic recovery, and self-healing for different applications. Further investigation into the relationship between polymer chain configuration and mechanical response like using labeled monomers[96] could help deepen the understanding of these elastomers.

Author contributions

H. Cai contributed to the investigation, methodology, writing-original draft, writing-review and editing, visualization. Z. Wang contributed to the methodology, writing-review and editing. N. W. Utomo contributed to the investigation and writing-review and editing. Y. Vidavsky contributed to the conceptualization, investigation, writing-review and editing, and funding acquisition. M.

N. Silberstein contributed to the conceptualization, project administration, supervision, writing-review and editing, and funding acquisition.

Conflicts of interest

The authors declare no conflicts of interest.

Acknowledgements

This work was supported by the U.S. Department of Energy, Office of Science, Basic Energy Sciences, under Award # DE-SC0019141. This work made use of the Cornell Center for Materials Research Shared Facilities which are supported through the NSF MRSEC program (DMR-1719875). This work made use of the Cornell University NMR Facility, which is supported, in part, by the NSF through MRI award CHE-1531632. We also want to express our gratitude to Max Tepermeister for his work in measuring the conductivity of our materials.

Notes and references

1 C. Goodyear, *Improvement in India Rubber Fabrics*, 1844.
2 A. Y. Coran, *Journal of Applied Polymer Science*, 2003, **87**, 24–30.
3 M. Akiba and A. S. Hashim, *Progress in Polymer Science*, 1997, **22**, 475–521.
4 Leslie H. Sperling, *Introduction to Physical Polymer Science*, Wiley, New Jersey, 4th edn, 2005.
5 Y. Liu, J. Chen, G. Li, X. Liu, X. Liao and Q. Yang, *J. Appl. Polym. Sci*, 2014, **131**, 40917.
6 S. Lin, J. Ni, D. Zheng and X. Zhao, *Extreme Mechanics Letters*, 2021, **48**, 101399.
7 T. Colclough, J. I. Cunneen and G. M. C. Higgins, *Journal of Applied Polymer Science*, 1968, **12**, 295–307.
8 S. Mitra, A. Ghanbari-Siahkali, P. Kingshott, H. K. Rehmeier, H. Abildgaard and K. Almdal, *Polymer Degradation and Stability*, 2006, **91**, 69–80.
9 C. S. Schollenberger and K. Dinbergs, *Journal of Polymer Science: Polymer Symposium*, 1978, **64**, 351–368.
10 J. O. Akindoyo, M. D. H. Beg, S. Ghazali, M. R. Islam, N. Jeyaratnam and A. R. Yuvaraj, *RSC Advances*, 2016, **6**, 114453–114482.
11 R. J. Wojtecki, M. A. Meador and S. J. Rowan, *Nature Materials*, 2011, **10**, 14–27.
12 Z. Jiang, A. Bhaskaran, H. M. Aitken, I. C. G Shackleford and L. A. Connal, *Macromolecular Rapid Communications*, 2019, **40**, 1900038.
13 Y. Miwa, J. Kurachi, Y. Kohbara and S. Kutsumizu, *Communications Chemistry*, 2018, **1**, 1–8.
14 Y. Peng, Y. Yang, Q. Wu, S. Wang, G. Huang and J. Wu, *Polymer*, 2018, **157**, 172–179.
15 C. H. Li, C. Wang, C. Keplinger, J. L. Zuo, L. Jin, Y. Sun, P. Zheng, Y. Cao, F. Lissel, C. Linder, X. Z. You and Z. Bao, *Nature Chemistry*, 2016, **8**, 618–624.
16 X. Zhang, Y. Vidavsky, S. Aharonovich, S. J. Yang, M. R. Buche, C. E. Diesendruck and M. N. Silberstein, *Soft Matter*, 2020, **16**, 8591–8601.
17 Y. Vidavsky, S. Bae and M. N. Silberstein, *Journal of Polymer Science, Part A: Polymer Chemistry*, 2018, **56**, 1117–1122.
18 Y. Vidavsky, M. R. Buche, Z. M. Sparrow, X. Zhang, S. J. Yang, R. A. Distasio and M. N. Silberstein, *Macromolecules*, 2020, **53**, 2021–2030.
19 G. E. Sanoja, N. S. Schauser, J. M. Bartels, C. M. Evans, M. E. Helgeson, R. Seshadri and R. A. Segalman, *Macromolecules*, 2018, **51**, 2017–2026.
20 D. K. Hohl, A. C. Ferahian, L. Montero De Espinosa and C. Weder, *ACS Macro Letters*, 2019, **8**, 1484–1490.
21 B. A. Lamers, M. L. Ślczkowski, F. Wouters, T. A. Engels, E. W. Meijer and A. R. Palmans, *Polymer Chemistry*, 2020, **11**, 2847–2854.
22 Z. Xie, B. L. Hu, R. W. Li and Q. Zhang, *ACS Omega*, 2021, **6**, 9319–9333.
23 E. Su, M. Yurtsever and O. Okay, *Macromolecules*, 2019, **52**, 3257–3267.
24 G. M. Scheutz, J. J. Lessard, M. B. Sims and B. S. Sumerlin, *Journal of the American Chemical Society*, 2019, **141**, 16181–16196.
25 P. Chakma and D. Konkolewicz, *Angewandte Chemie*, 2019, **131**, 9784–9797.
26 T. Shen, Z. Song, S. Cai and F. J. Vernerey, *Proceedings of the National Academy of Sciences of the United States of America*, 2021, **118**, e2105974118.
27 X. Kuang, S. Wu, Q. Ze, L. Yue, Y. Jin, S. M. Montgomery, F. Yang, H. J. Qi and R. Zhao, *Advanced Materials*, 2021, **33**, 2102113.
28 S. Y. Son, J.-H. Kim, E. Song, K. Choi, J. Lee, K. Cho, T.-S. Kim and T. Park, *Macromolecules*, 2018, **51**, 2572–2579.
29 H. Fan, J. Wang, Z. Tao, J. Huang, P. Rao, T. Kurokawa and J. P. Gong, *Nature Communications*, 2019, **10**, 5127.
30 S. Zhao, D. Wang and T. P. Russell, *ACS Sustainable Chemistry and Engineering*, 2021, **9**, 11091–11099.
31 W. Niu, X. Cao, Y. Wang, B. Yao, Y. Zhao, J. Cheng, S. Wu, S. Zhang and X. He, *Advanced Functional Materials*, 2021, **31**, 2009017.
32 J. Y. Sun, X. Zhao, W. R. Illeperuma, O. Chaudhuri, K. H. Oh, D. J. Mooney, J. J. Vlassak and Z. Suo, *Nature*, 2012, **489**, 133–136.
33 S. Salaeh, A. Das and S. Wießner, *Polymer*, 2021, **223**, 123699.
34 C. Lu, Y. Liu, X. Liu, C. Wang, J. Wang and F. Chu, *ACS Sustainable Chemistry and Engineering*, 2018, **6**, 6527–6535.
35 Y. Zhang, Q. Hu, S. Yang, T. Wang, W. Sun and Z. Tong, *Macromolecules*, 2021, **54**, 5218–5228.
36 W. Zhang, M. Wang, J. Zhou, Y. Sheng, M. Xu, X. Jiang, Y. Ma and X. Lu, *European Polymer Journal*, 2021, **156**, 110614.
37 A. J. R. Amaral and G. Pasparakis, *Polymer Chemistry*, 2017, **8**, 6464–6484.
38 J. Dahlke, S. Zechel, M. D. Hager and U. S. Schubert, *Advanced Materials Interfaces*, 2018, **5**, 1800051.
39 Y. Chen, Z. Tang, Y. Liu, S. Wu and B. Guo, *Macromolecules*, 2019, **52**, 3805–3812.

40 A. M. Wemyss, C. Bowen, C. Plesse, C. Vancaeyzeele, G. T. Nguyen, F. Vidal and C. Wan, *Materials Science and Engineering: R: Reports*, 2020, **141**, 100561.

41 Y. Gao, J. Chen, X. Han, Y. Pan, P. Wang, T. Wang and T. Lu, *Advanced Functional Materials*, 2020, **30**, 2003207.

42 X. Chen, H. Yuk, J. Wu, C. S. Nabzdyk and X. Zhao, *Proceedings of the National Academy of Sciences of the United States of America*, 2020, **117**, 15497–15503.

43 Z. Chen, M. Yang, M. Ji, X. Kuang, H. J. Qi and T. Wang, *Materials and Design*, 2021, **197**, 109189.

44 F. Zhu, L. Cheng, J. Yin, Z. L. Wu, J. Qian, J. Fu and Q. Zheng, *ACS Applied Materials and Interfaces*, 2016, **8**, 31304–31310.

45 J. Chen, J. Huang and Y. Hu, *ACS Applied Materials and Interfaces*, 2021, **13**, 12726–12734.

46 X. Zhang, R. Crisci, J. A. Finlay, H. Cai, A. S. Clare, Z. Chen and M. N. Silberstein, *Advanced Materials Interfaces*, 2022, **9**, 2200430.

47 Y. Chen, H. Zhang, J. Chen, G. Kang and Y. Hu, *Acta Mechanica Sinica*, 2021, **37**, 748–756.

48 N. Yoshie, M. Watanabe, H. Araki and K. Ishida, *Polymer Degradation and Stability*, 2010, **95**, 826–829.

49 S. Ji, W. Cao, Y. Yu and H. Xu, *Advanced Materials*, 2015, **27**, 7740–7745.

50 Y. Miwa, K. Taira, J. Kurachi, T. Udagawa and S. Kutsumizu, *Nature Communications*, 2019, **10**, 1828.

51 Z. Yu, D. G. Mackanic, W. Michaels, M. Lee, A. Pei, D. Feng, Q. Zhang, Y. Tsao, C. V. Amanchukwu, X. Yan, H. Wang, S. Chen, K. Liu, J. Kang, J. Qin, Y. Cui and Z. Bao, *Joule*, 2019, **3**, 2761–2776.

52 Y. Lin, Y. Chen, Z. Yu, Z. Huang, J.-C. Lai, J. B-H Tok, Y. Cui and Z. Bao, *Chemistry of Materials*, 2022, **34**, 2393–2399.

53 W. J. Zheng, N. An, J. H. Yang, J. Zhou and Y. M. Chen, *ACS Applied Materials and Interfaces*, 2015, **7**, 1758–1764.

54 Y. Cheng, K. Hoe Chan, X.-Q. Wang, T. Ding, T. Li, C. Zhang, W. Lu, Y. Zhou and G. Wei Ho, *Advanced Functional Materials*, 2021, **31**, 2101825.

55 Y. Guo, S. Chen, L. Sun, L. Yang, L. Zhang, J. Lou and Z. You, *Advanced Functional Materials*, 2020, **31**, 2009799.

56 H. Wang and S. C. Heilshorn, *Advanced Materials*, 2015, **27**, 3717–3736.

57 L. Saunders and P. X. Ma, *Macromolecular Rapid Communications*, 2019, **19**, 1800313.

58 T. L. Sun, T. Kurokawa, S. Kuroda, A. B. Ihsan, T. Akasaki, K. Sato, M. A. Haque, T. Nakajima and J. P. Gong, *Nature Materials*, 2013, **12**, 932–937.

59 F. Luo, T. L. Sun, T. Nakajima, T. Kurokawa, Y. Zhao, K. Sato, A. B. Ihsan, X. Li, H. Guo and J. P. Gong, *Advanced Materials*, 2015, **27**, 2722–2727.

60 F. Luo, T. L. Sun, T. Nakajima, T. Kurokawa, A. B. Ihsan, X. Li, H. Guo and J. P. Gong, *ACS Macro Letters*, 2015, **4**, 961–964.

61 K. Cui, T. L. Sun, T. Kurokawa, T. Nakajima, T. Nonoyama, L. Chen and J. P. Gong, *Soft Matter*, 2016, **12**, 8833–8840.

62 M. Criado-Gonzalez, D. Wagner, J. Rodon Fores, C. Blanck, M. Schmutz, A. Chaumont, M. Rabineau, J. B. Schlenoff, G. Fleith, J. Combet, P. Schaaf, L. Jierry and F. Boulmedais, *Chemistry of Materials*, 2020, **32**, 1946–1956.

63 F. B. Madsen, L. Yu and A. L. Skov, *ACS Macro Letters*, 2016, **5**, 1196–1200.

64 S. Zheng, Y. Chen and M. A. Brook, *Polymer Chemistry*, 2020, **11**, 7382–7392.

65 H. Zhang, Y. Wu, J. Yang, D. Wang, P. Yu, C. To Lai, A.-C. Shi, J. Wang, S. Cui, J. Xiang, N. Zhao and J. Xu, *Advanced Materials*, 2019, **31**, 1904029.

66 P. Schaaf and J. B. Schlenoff, *Advanced Materials*, 2015, **27**, 2420–2432.

67 Q. Wang and J. B. Schlenoff, *Macromolecules*, 2014, **47**, 3108–3116.

68 A. Reisch, E. Roger, T. Phoeung, C. Antheaume, C. Orthlieb, F. Boulmedais, P. Lavalle, J. B. Schlenoff, B. Frisch and P. Schaaf, *Advanced Materials*, 2014, **26**, 2547–2551.

69 G. Rydzek, A. Pakdel, A. Witecka, D. N. Awang Shri, F. Gaudière, V. Nicolosi, P. Mokarian-Tabari, P. Schaaf, F. Boulmedais and K. Ariga, *Macromolecules*, 2018, **51**, 4424–4434.

70 R. Saikaew, W. Meesorn, J. O. Zoppe, C. Weder and S. T. Dubas, *Macromolecular Materials and Engineering*, 2019, **304**, 1900245.

71 L. Yu, F. B. Madsen, S. Hvilsted and A. L. Skov, *RSC Advances*, 2015, **5**, 49739–49747.

72 S. Li, H. Pan, Y. Wang and J. Sun, *Journal of Materials Chemistry A*, 2020, **8**, 3667–3675.

73 A. E. Neitzel, Y. N. Fang, B. Yu, A. M. Rumyantsev, J. J. de Pablo and M. V. Tirrell, *Macromolecules*, 2021, **54**, 6878–6890.

74 A. M. Rumyantsev, N. E. Jackson and J. J. De Pablo, *Annual Review of Condensed Matter Physics*, 2021, **12**, 155–176.

75 S. Shah and L. Leon, *Current Opinion in Colloid & Interface Science*, 2021, **53**, 101424.

76 S. Gao, A. Holkar and S. Srivastava, *Polymers*, 2019, **11**, 1097.

77 J. Li, H. Zhu, X. Wang, M. Armand, D. R. Macfarlane and M. Forsyth, *Electrochimica Acta*, 2015, **175**, 232–239.

78 L. Zhang, N. R. Brostowitz, K. A. Cavicchi and R. A. Weiss, *Macromolecular Reaction Engineering*, 2014, **8**, 81–99.

79 H. H. Hariri, A. M. Lehaf and J. B. Schlenoff, *Macromolecules*, 2012, **45**, 9364–9372.

80 S. Belfer, Y. Purinson, R. Fainshtein, Y. Radchenko and O. Kedem, *Acta Polymerica*, 1998, **49**, 574–582.

81 F. Cabassi, B. Casu and A. S. Perlin, *Carbohydrate Research*, 1978, **63**, 1–11.

82 *Plastics Technology*, 2022, `http://polymerdatabase.com/main.html`.

83 W. Imre, M. Schönhoff and C. Cramer, *Journal of Chemical Physics*, 2008, **128**, 134905.

84 A. Vidyasagar, C. Sung, R. Gamble and J. L. Lutkenhaus, *ACS Nano*, 2012, **6**, 6174–6184.

85 L. A. Wood, *Journal of Polymer Science*, 1958, **XXVIII**, 319–330.

86 M. Bellinger, J. A. Sauer and M. Hara, *Macromolecules*, 1994, **27**, 1407–1412.

87 O. Jaudouin, J. J. Robin, J. M. Lopez-Cuesta, D. Perrin and C. Imbert, *Polymer International*, 2012, **61**, 495–510.
88 L. Andreozzi, V. Castelvetro, M. Faetti, M. Giordano and F. Zulli, *Macromolecules*, 2006, **39**, 1880–1889.
89 R. Bai, Q. Yang, J. Tang, X. P. Morelle, J. Vlassak and Z. Suo, *Extreme Mechanics Letters*, 2017, **15**, 91–96.
90 L. Leibler, M. Rubinstein and R. H. Colby, *Macromolecules*, 1991, **24**, 4701–4707.
91 R. Long, K. Mayumi, C. Creton, T. Narita and C.-Y. Hui, *Macromolecules*, 2014, **47**, 7243–7250.
92 Y. Mao, S. Lin, X. Zhao and L. Anand, *Journal of the Mechanics and Physics of Solids*, 2017, **100**, 103–130.
93 S. C. Lamont, J. Mulderrig, N. Bouklas and F. J. Vernerey, *Macromolecules*, 2021, **54**, 10801–10813.
94 S. K. Sukumaran, G. Beaucage, J. E. Mark and B. Viers, *European Physical Journal E*, 2005, **18**, 29–36.
95 T. Karino, M. Shibayama, Y. Okumura and K. Ito, *Physica B: Condensed Matter*, 2006, **385-386**, 807–809.
96 J. Früh, R. Köhler, H. Möhwald and R. Krastev, *Langmuir*, 2010, **26**, 15516–15522.
97 J. Frueh, A. Rühm, Q. He, H. Möhwald, R. Krastev and R. Köhler, *Langmuir*, 2018, **34**, 11933–11942.